nanomaterials

MDPI

Article

Sonochemical Synthesis of Copper-doped $BiVO_4$/g-C_3N_4 Nanocomposite Materials for Photocatalytic Degradation of Bisphenol A under Simulated Sunlight Irradiation

Gang-Juan Lee [1], Xin-Yu Lee [1], Cong Lyu [2], Na Liu [2], Sambandam Andandan [3] and Jerry J. Wu [1,*]

1 Department of Environmental Engineering and Science, Feng Chia University, Taichung 407, Taiwan; leeganjiuan@gmail.com (G.-J.L.); chatter850603@gmail.com (X.-Y.L.)
2 College of New Energy and Environment, Jilin University, Changchun 130021, China; lvcong@jlu.edu.cn (C.L.); liuna@jlu.edu.cn (N.L.)
3 Nanomaterials & Solar Energy Conversion Lab, Department of Chemistry, National Institute of Technology, Trichy 620015, India; sanand@nitt.edu
* Correspondence: jjwu@mai.fcu.edu.tw; Tel.: +886-4-24517250 (ext. 5206); Fax: +886-4-24517686

Received: 12 February 2020; Accepted: 5 March 2020; Published: 10 March 2020

Abstract: Copper-doped bismuth vanadate/graphitic carbon nitride ($BiVO_4$/g-C_3N_4) nanocomposite materials were successfully fabricated using a sonochemical approach. Cu-doped $BiVO_4$/g-C_3N_4 nanocomposite photocatalysts could improve electron/hole (e^-/h^+) pair separation, stability, and light-harvesting efficiency compared to pristine $BiVO_4$ or g-C_3N_4, resulting in the enhancement of photocatalytic activity. The optimal parameters, such as pH value at 10, photocatalyst dosage of 0.4 g L^{-1}, and 10 mol% Cu-doped $BiVO_4$/g-C_3N_4 photocatalyst, were determined to degrade initial concentration of 20 ppm Bisphenol A, which could be completely removed after 90 min. Furthermore, the excessive doping of copper (> 10 mol%) could not synthesize the pure monoclinic scheelite phase, which substantially resulted in the reduction of the photocatalytic activity.

Keywords: sonochemical synthesis; composite nanomaterials; photocatalytic degradation

1. Introduction

Bismuth vanadate ($BiVO_4$) has three crystal phases, such as tetragonal-scheelite, monoclinic scheelite, and zircon. Among those, the monoclinic phase, in particular, exhibits outstanding visible-light photocatalytic properties because monoclinic scheelite $BiVO_4$ possesses the small bandgap 2.4 eV [1–5]. Dong et al. (2016) [6] prepared monoclinic scheelite $BiVO_4$ semiconductors with porous structures using a two-step method. The porous $BiVO_4$ material prepared at hydrothermal temperatures of 200 °C displays enhanced photocatalytic efficiency by degrading methylene blue (MB). Sun et al. (2019) revealed that the two-dimensional $BiVO_4$ nanosheets/reduced graphene oxide (RGO) exhibited higher photocatalytic activity [7]. In addition, the heterojunction of semiconductor composite has been reported to be an effective strategy to fabricate efficient photocatalysts [6]. Xie et al. (2018) exhibited that the $BiVO_4$/Mn-Zn ferrite ($Mn_{1-x}Zn_xFe_2O_4$)/RGO photocatalyst could degrade rhodamine B (RhB) about 96% [8]. Thus, in this article, we chose graphitic carbon nitride (g-C_3N_4) to modify $BiVO_4$ to enhance photocatalytic efficiency due to graphene-like structure, good thermal and chemical stability, good visible light absorption, and photocatalytic properties of g-C_3N_4 [6]. In addition, g-C_3N_4 nanosheets could enhance an easier electron transfer during the reaction [9]. Smykalova et al. (2019) indicated that g-C_3N_4 nanosheets possessed a large specific surface area, which

resulted in the higher degradation ratio of medicines in water [10]. Zhang et al. (2017) indicated that the composite with 7 wt% g-C_3N_4 had better photocatalytic efficiency than bare $BiVO_4$ [11]. The stable core/shell structure of the $BiVO_4$/g-C_3N_4 composite material not only enlarges the surface area but also enhances the photo-generated charge separation. Therefore, a new composite photocatalyst is expected to improve the stability, solar light utilization, charge separation, and transfer by combining with the two semiconductors.

BPA (bisphenol A) is not only a synthetic organic chemical with various applications in the polymer industry used as intermediate for the production of epoxy resins and plastics but also an endocrine disruptor, which would lead to serious ecology exacerbation [12,13]. Some researchers have shown that exposure to very low BPA levels may result in reduced fertility and increased incidence of breast, ovarian, and testicular cancers [13]. Therefore, BPA should be completely removed from the water for safety consideration to human beings. In this research, we prepared the $BiVO_4$ nanocomposite photocatalysts at 60 °C, 1 atm, and 1.5 h via a sonochemical synthesis way. The advantage of sonochemistry in fabricating nanostructured samples occurs mostly from acoustic cavitation [14]. In addition, we also introduced the synthesis of copper and g-C_3N_4-modified $BiVO_4$ and removal of BPA using photocatalytic reaction under simulated sunlight irradiation. Some parameters that affect the efficiency of BPA removal via the photocatalytic degradation process, including the pH values in solution, the dosages of $BiVO_4$ nanocomposite material, and the various $BiVO_4$ nanocomposite materials, were studied.

2. Methods

2.1. Sonochemical Synthesis of $BiVO_4$ Nanocomposite Photocatalysts

A total of 5 g urea (NH_2CONH_2, NIHON SHIYAKU REAGENT) was added into an aluminum crucible, and subsequent thermal treatment at 550 °C for 2 h with 5 °C min^{-1} of heating rate in argon atmosphere could obtain a light-yellow powder composed of g-C_3N_4 nanoparticles. A total of 3.38 g bismuth (III) nitrate pentahydrate ($Bi(NO_3)_3{\cdot}5H_2O$, Alfa Aesar) was placed in 40 mL of 2 M nitric acid solution (solution A). Then, 0-40 wt% g-C_3N_4 was put into solution A to be stirred for 1 h. The 0.81 g ammonium metavanadate (NH_4VO_3, Acros) was dissolved in 40 mL of deionized (DI) water (solution B). The 1 wt% surfactant, such as citric acid monohydrate (CIT, $C_6H_8O_7{\bullet}H_2O$, fw: 192.12, SHOWA), (1-hexadecyl)trimethylammonium bromide (CTAB, $CH_3(CH_2)_{15}N(CH_3)_3Br$, fw: 364.42, Alfa Aesar), and polyethylene glycol (PEG, $C_{2n}H_{4n+2}O_{n+1}$, fw: 4,000, SHOWA), was added into the solution B. The 0-20 mol% copper (II) acetate monohydrate ($Cu(CH_3COO)_2{\bullet}H_2O$, Merck) was also added in 20 mL of DI water (solution C). Subsequently, solution A and solution C were added into solution B. Then, the reaction mixture was treated with a sonochemical instrument (700 W, 20 kHz, Q700 SONICATOR) for 0.5 h–2 h at 60 °C [4]. Finally, the copper-doped $BiVO_4$/g-C_3N_4 samples were collected.

2.2. Characterization of $BiVO_4$ Nanocomposite Photocatalysts

The morphologies were examined by the JEOL JSM-7800F model and the JEOL JEM-2010 model. The XRD patterns were examined by the Rigaku Ultima III diffractometer (Rigaku Japan Sales Division, Tokyo, Japan). Particle size distribution, bandgap, and photoluminescence (PL) properties were measured using the Shimadzu SALD-2300 model, Shimadzu UV-2600 and Shimadzu RF-3501 spectrometer (Shimadzu Corporation, Tokyo, Japan), respectively. The flat-band potential of the sample was recorded using potentiostat/galvanostat PGSTAT302N, Metrohm Autolab (Metrohm AG, Herisau, Switzerland). The surface area, pore size, and pore volume were measured by using a Micrometrics ASAP-2020 nitrogen adsorption instrument (Micrometrics Headquarters, Norcross, GA, USA).

2.3. Photocatalytic Reaction

Typically, an appropriate amount of $BiVO_4$ nanocomposite material was put into 100 mL of BPA solution (4,4'-dihydroxy-2,2-diphenylpropane, Bisphenol A, $C_{15}H_{16}O_2$, ECHO) with a concentration

of 20 ppm. The reactor was irradiated with a 350 W Xenon light (KIT-XENON-ADJ350W) for 6 h. During the experiment, about 1.5 mL sample was withdrawn at predetermined time intervals, and the sample was immediately filtered through the 0.22 μm polyvinylidene difluoride (PVDF) syringe filter to remove the powders, and the clarified solution was analyzed by High-performance liquid chromatography (HPLC, LC-20A, Shimadzu Corporation, Tokyo, Japan).

3. Results

3.1. Characterization of $BiVO_4$ Nanocomposite Photocatalysts

Reaction conditions could effectively affect the morphology of photocatalysts. Figure 1a–d show when irradiation time was extended, the particle size of $BiVO_4$ nanoparticles could gradually enlarge. As time was irradiated for 1.5 h, $BiVO_4$ samples had the uniform particle size and the rough surface. The phase and crystallographic nanostructures of the $BiVO_4$ particles are shown in Figure 1e. The major diffraction peaks at 18.83°, 28.84°, 30.56°, 34.51°, 35.22°, 39.96°, 42.40°, 45.84°, 46.74°, 47.25°, 50.28°, and 53.22° belonged to the (011), (121), (040), (200), (002), (211), (051), (132), (240), (042), (202), and (161) planes of $BiVO_4$ nanostructures and matched well with the crystal phase of monoclinic $BiVO_4$ (JCPDS Card No. 14-0688, cell parameter a = 5.195 Å, b = 11.70 Å, and c = 5.092 Å). No other impurities could be detected. This also indicated that the ultrasonic time did not influence the crystal structure. According to our previous study, surfactant would affect the formation of various morphological structures [15]. Therefore, we used three types of surfactants to control the particle size of $BiVO_4$, such as CIT (chelating agent), CTAB (cationic surfactant), and PEG (non-ionic surfactant). Figure 1f–h show FE-SEM images and particle size distribution of $BiVO_4$ with various surfactants. The particle size distribution (D_{50}) of $BiVO_4$ with surfactants significantly decreased from 11.971 μm to 0.330 μm, which could be attributed to better dispersibility by adding the surfactants with long molecular chain and hydrophilic end during the synthetic process [16–18]. Therefore, the smaller particle size could be formed than that of pristine $BiVO_4$.

The $BiVO_4$ photocatalyst was further modified by g-C_3N_4 and copper in order to promote the photocatalytic activity. The results were confirmed by HR-TEM measurement on the 10Cu/$BiVO_4$/g-C_3N_4 powders (Figure 2). The corresponding selected area electron diffraction (SAED) pattern indicated rings; the as-synthesized $BiVO_4$ nanocomposite photocatalysts was the polycrystalline structure (Figure 2b). Furthermore, the element of Bi, V, O, C, N, and Cu substantially existed in the sample from the EDX image and TEM-EDX element mapping (Figure 2c–i). The bandgap of g-C_3N_4 and copper-modified $BiVO_4$ slightly reduced from 2.47 eV to 2.28 eV (Figure 3a). The PL spectra of the $BiVO_4$ samples are exhibited in Figure 3b. $BiVO_4$ photocatalyst displayed two peaks at 530.7 nm and 357.7 nm [19]. The g-C_3N_4 had its characteristic peak around at 450.4 nm [20]. In addition, the pristine $BiVO_4$ sample had higher PL intensity than that of g-C_3N_4 and copper-modified $BiVO_4$ samples. In other words, the e^-/h^+ recombination rate could be efficiently restrained in the g-C_3N_4 and Cu-modified $BiVO_4$ samples. In the high concentration of copper (> 10 mol%), the PL peak of $BiVO_4$ nanocomposite photocatalysts shifted from 530.7 nm to 492.7–469.4 nm due to the fabrication of the tetragonal-scheelite structure $BiVO_4$, as shown in Figure 4. Therefore, the excessive doping of copper (> 10 mol%) could not synthesize the pure monoclinic scheelite phase, which might result in the reduction of the photocatalytic activity.

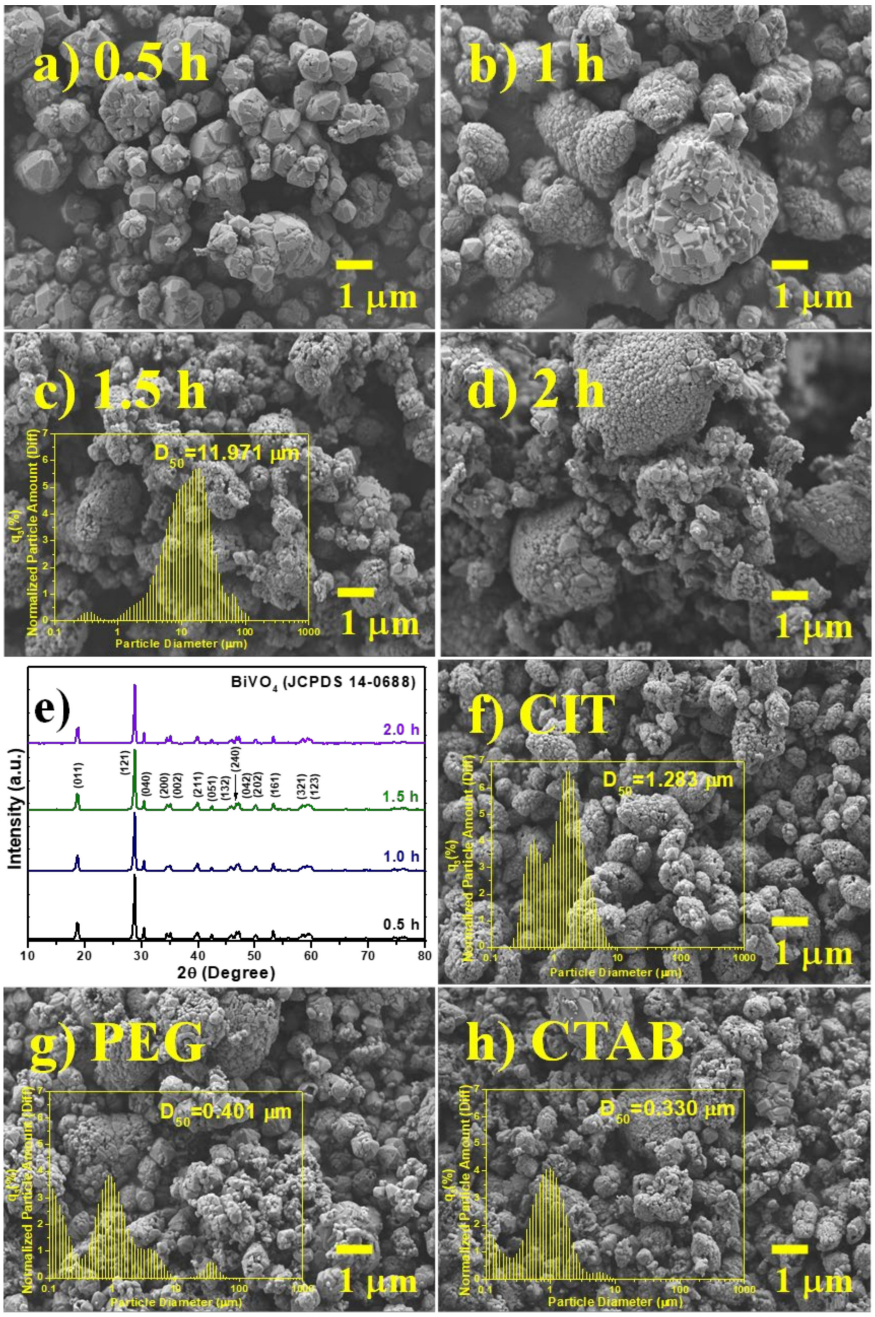

Figure 1. FESEM images (**a**–**d**), and XRD patterns (**e**) of $BiVO_4$ photocatalysts with different ultrasound irradiation time (without surfactant). FESEM images (**f**–**h**) of $BiVO_4$ materials via various surfactants at 1 wt%. Insets reveal the particle size distribution for the corresponding samples.

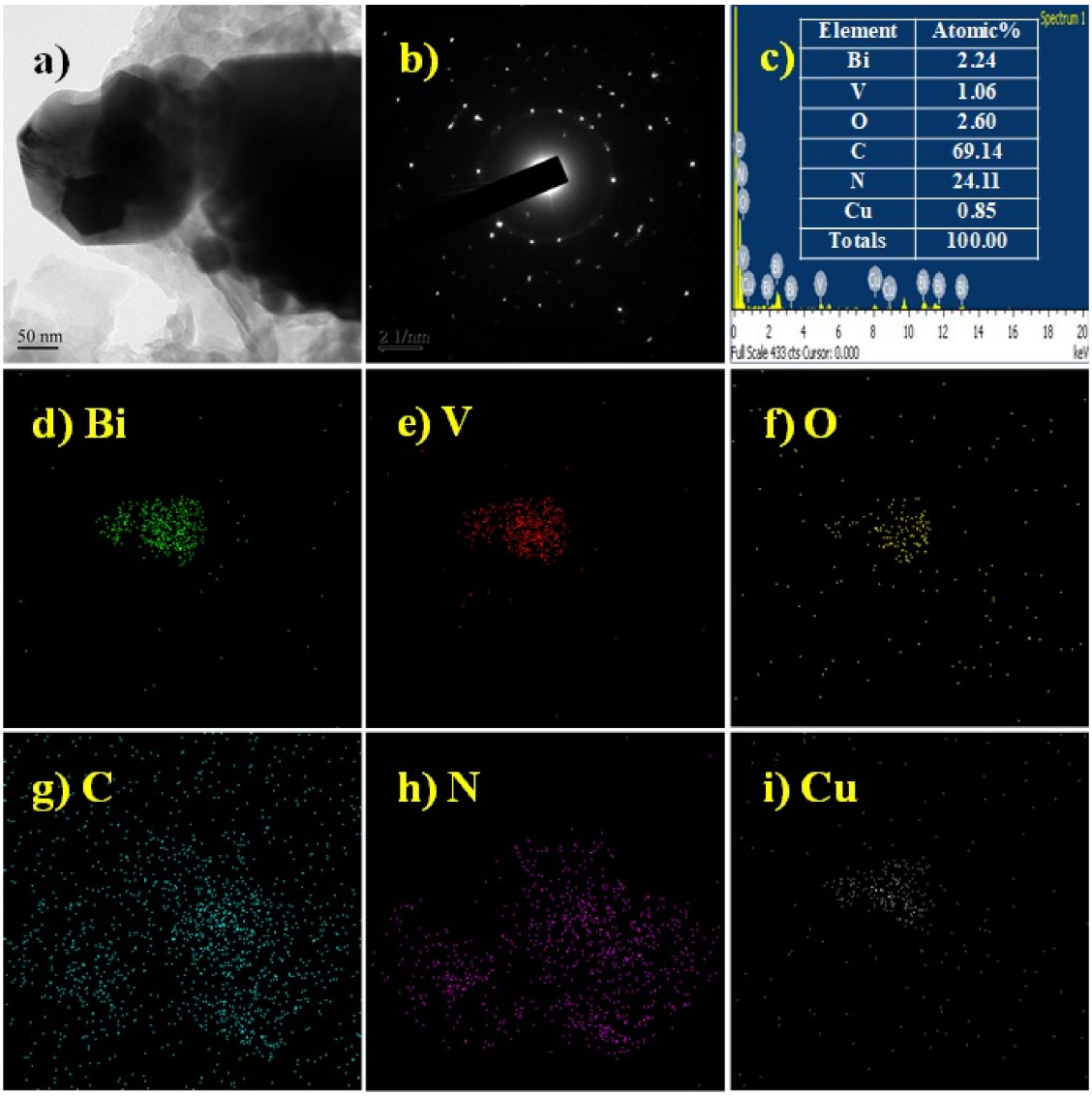

Figure 2. Typical TEM image (**a**), corresponding selected area electron diffraction (SAED) pattern (**b**), EDX (**c**), and elemental mapping record Bi, V, O, C, N, and Cu (**d**–**i**) of the 10Cu/$BiVO_4$/g-C_3N_4.

3.2. Photocatalytic Degradation Activity

The photocatalytic degradation activities of the $BiVO_4$ nanocomposite photocatalysts were performed for the degradation of wastewater pollutants containing BPA under simulated sunlight irradiation. Photocatalytic parameters of degrading BPA were investigated as below, including the pH values of BPA solution, the dosages of $BiVO_4$ nanocomposite photocatalyst, and the content of copper.

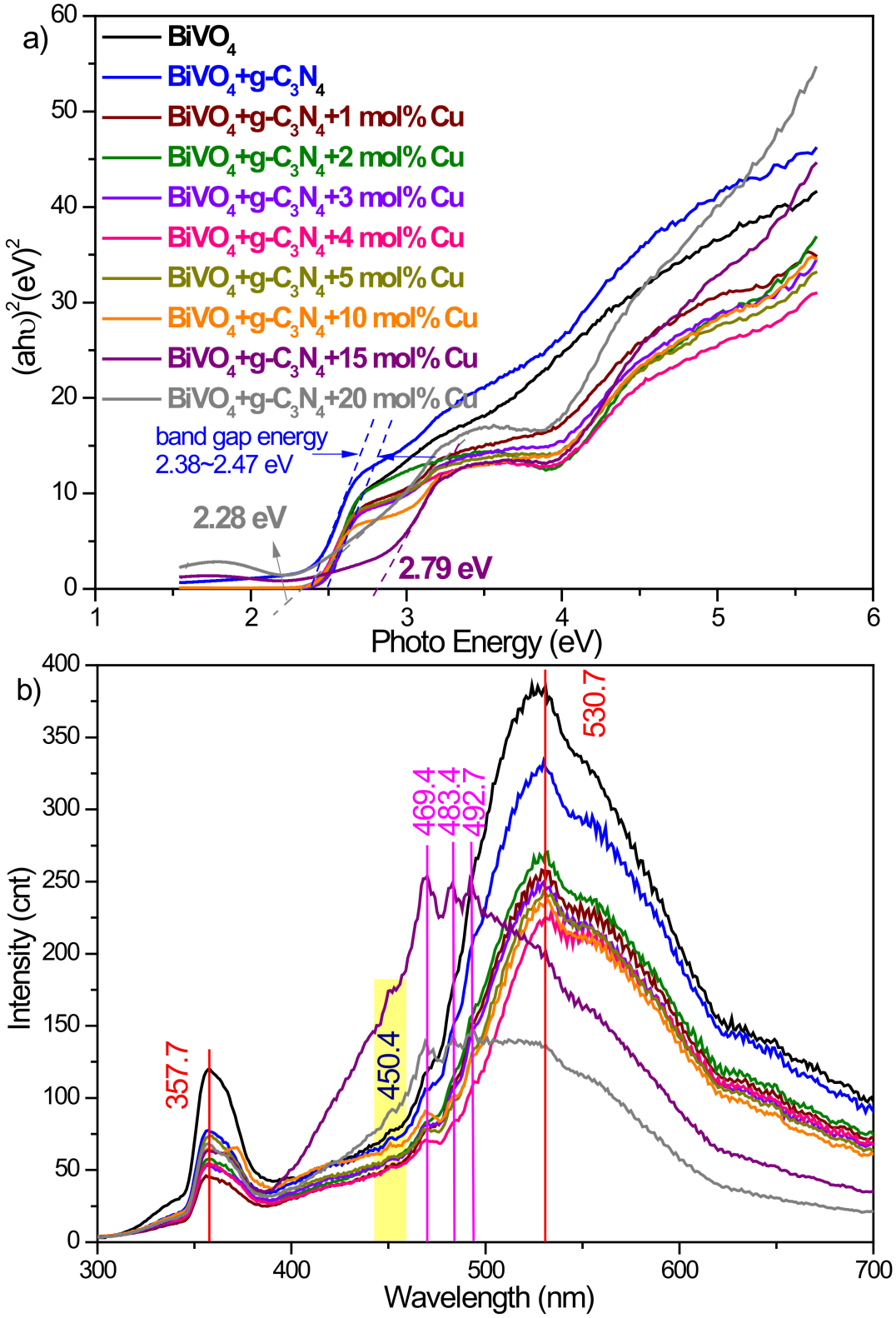

Figure 3. (**a**) UV-Vis absorption spectra, and (**b**) photoluminescence spectra of $BiVO_4$/g-C_3N_4 nanocomposite materials with various amounts of copper.

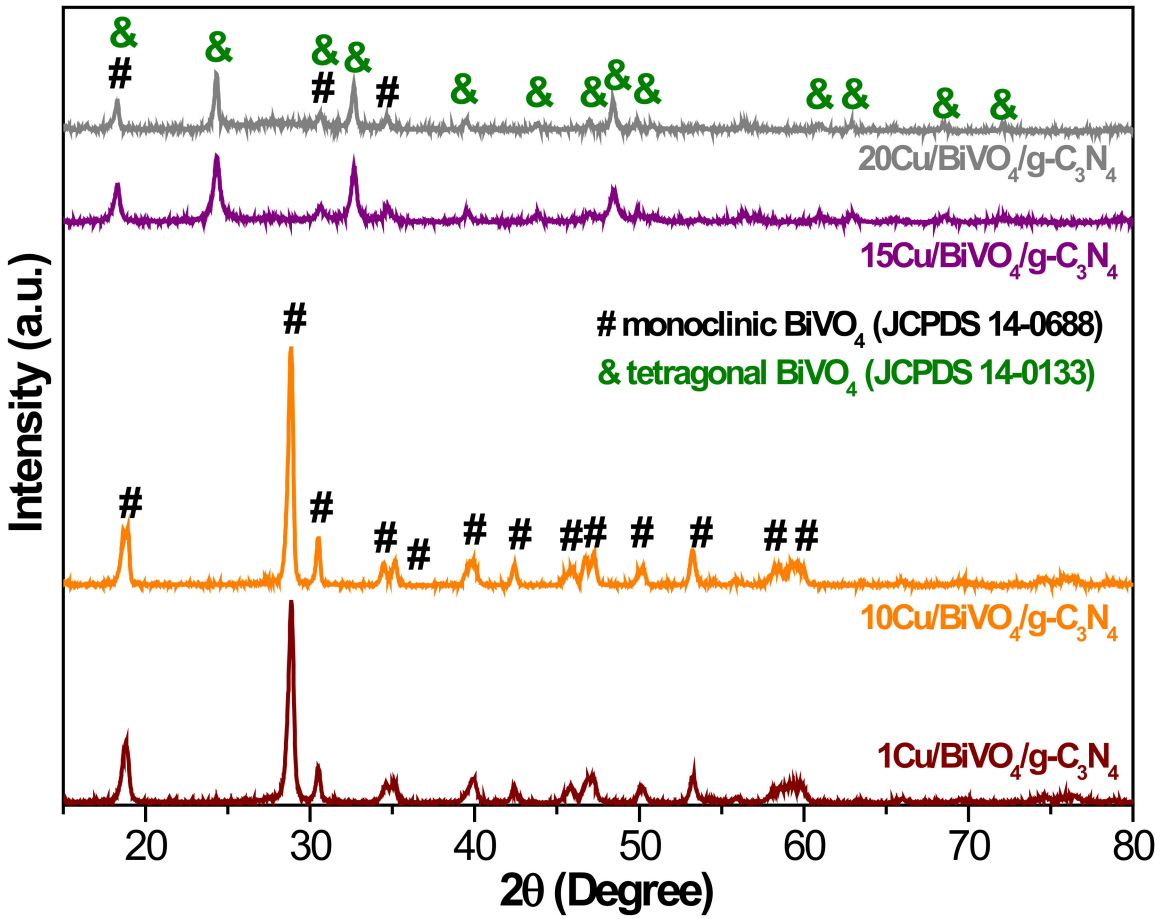

Figure 4. XRD patterns of $BiVO_4$/g-C_3N_4 nanocomposite materials with various amounts of copper.

3.2.1. Initial pH of the BPA Solution

Figure 5a plots the photo-degradation of BPA at various pH values. The results could be well fitted by pseudo-first-order kinetics model with a rate constant of 0.0036 min^{-1}, 0.0034 min^{-1}, 0.0072 min^{-1}, 0.0426 min^{-1}, and 0.0053 min^{-1} for pH value of 4, 7, 9, 10, and 12, respectively. With the increase of the pH value to 10, the BPA could be completely removed to 100% for 120 min. This result could be illustrated by the net signs of the surface charge of the BPA species and $BiVO_4$ nanocomposite photocatalysts at different pH values. Because the dissociation constants (pK_{a1} and pK_{a2}) of BPA are 9.6 and 10.2 [21–23], the surface charge of the BPA species is negatively charged under alkaline conditions. In addition, the pH changes also could affect the surface properties of 10Cu/$BiVO_4$/g-C_3N_4 photocatalyst. Meanwhile, we measured the point of zero charge of 10Cu/$BiVO_4$/g-C_3N_4 photocatalyst (pH_{pzc} = 11.3). Therefore, BPA molecules were adsorbed onto the surface of 10Cu/$BiVO_4$/g-C_3N_4 photocatalyst via electrostatic interaction (pH smaller than 11.3), which is an important step in the process of photocatalytic degradation. Conversely, BPA was adsorbed weakly onto the negatively charged 10Cu/$BiVO_4$/g-C_3N_4 surfaces due to the coulombic repulsion (pH greater than 11.3). Based on the above results, the best pH value of the BPA solution for the photocatalytic degradation of BPA was at 10.

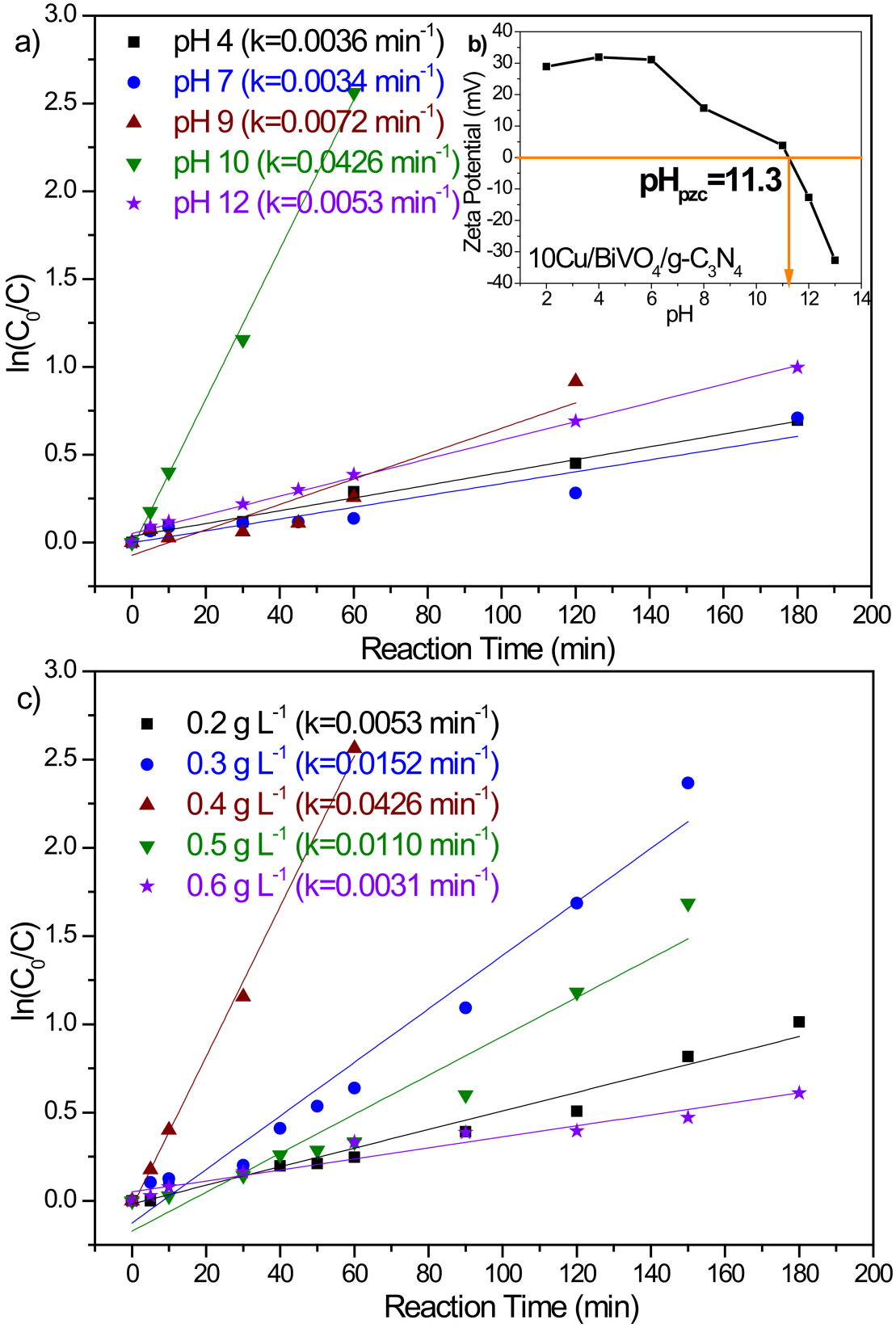

Figure 5. (**a**) Effect of bisphenol A (BPA) photodegradation at the different initial solution pH values on 10Cu/$BiVO_4$/g-C_3N_4 photocatalyst. ((BPA): 20 mg L^{-1}; catalyst concentration of 0.4 g L^{-1}), (**b**) The zeta potential values of 10Cu/$BiVO_4$/g-C_3N_4 photocatalyst, (**c**) Changes of the apparent BPA photodegradation reaction kinetics at a different dosage of 10Cu/$BiVO_4$/g-C_3N_4 photocatalyst. ((BPA): 20 mg L^{-1}; pH = 10).

3.2.2. Photocatalyst Dosage

The photocatalytic efficiency by using metal oxides can be determined by their physical and chemical properties. Physical properties, such as pore size, surface area, and surface charge, could affect the photocatalytic activity [24]. Therefore, the function of the photocatalysts is able to provide effective surface area and play the role of the active center. The effect of photocatalyst dosage on the degradation efficiency was evaluated by various amounts of 10Cu/$BiVO_4$/g-C_3N_4 from 0.2 g to 0.6 g in a 1000 mL BPA solution. The result of the photo-degradation performance has been depicted in Figure 5c, which exhibits that the rate of degradation increased linearly with an increase in the amount of photocatalyst up to 0.4 g and then decreased. The presence of 10Cu/$BiVO_4$/g-C_3N_4 photocatalyst could provide more active centers, which led to increased photocatalytic activity. As the amount of photocatalyst increased, the number of BPA molecules adsorbed were increased, leading to an increase in BPA degradation. At higher concentrations of photocatalyst, more surface areas were available for constant BPA molecules. However, more photocatalyst would also induce greater aggregation of the photocatalyst, and the specific surface area decreased, leading to a reduction in the reaction rate. In addition, the inactivation of activated molecules by collision with ground-state molecules might also hinder the photocatalytic efficiency. Hence, above a certain level, additional catalyst amounts were not involved in catalysis reaction, and thus the rate might level off. Hence, the appropriate photocatalyst dosage showed an outstanding performance of photocatalytic degradation.

3.2.3. Cu Doping Content

In view of the above results, we conducted the experiments of the photocatalytic degradation of BPA by $BiVO_4$ nanocomposite photocatalyst equal to 0.4 g L^{-1} at pH 10. Figure 6a exhibits the photocatalytic activity of $BiVO_4$ nanocomposite photocatalysts with various Cu contents. It could be seen that the Cu content in the $BiVO_4$ presented an excellent influence on the photocatalytic activity of $BiVO_4$ nanocomposite materials. The conduction band (CB) edge position and valence band (VB) edge position of bare $BiVO_4$ were about 0.75 eV and 3.22 eV, respectively, leading to a weak reduction ability, as shown in Figure 6b. The 10 mol% Cu-doped $BiVO_4$ photocatalyst could not only shift the CB edge position more negative than the others but also decrease the intensity of PL emission (Figure 3b). Therefore, 10Cu/$BiVO_4$/g-C_3N_4 photocatalyst had the highest activity (k = 0.0426 min^{-1}) for photocatalytic degradation. Moreover, the addition of excess Cu contents (> 10 mol%) to synthesize $BiVO_4$ nanocomposite photocatalysts resulted in a reduction in the photocatalytic activity because $BiVO_4$ formed the tetragonal-scheelite phase, as shown in Figure 4. According to the references, we know that the crystal structure of monoclinic type $BiVO_4$ exhibits excellent photocatalytic properties [2–4]. In addition, copper-doped photocatalyst can fabricate the trap energy levels (TEL), and the activated electrons could transfer to TEL_{Cu}, which leads to the useful e^-/h^+ separation [15,16,25–27]. Therefore, the appropriate addition of Cu contents displayed an excellent photocatalytic degradation performance. Furthermore, the 10Cu/$BiVO_4$/g-C_3N_4 was assigned to the type IV isotherm, displaying with a type H3 hysteresis loop, which indicated the presence of mesopores (2–50 nm), as shown in Figure 7. The $BiVO_4$/g-C_3N_4 nanocomposite materials with various amounts of copper addition are compared in Table 1, revealing a slight decrease in the surface areas with copper doping. However, the slight loss of specific surface area did not compete with the enhanced activity of doping copper as reaction centers for photocatalytic degradation of BPA.

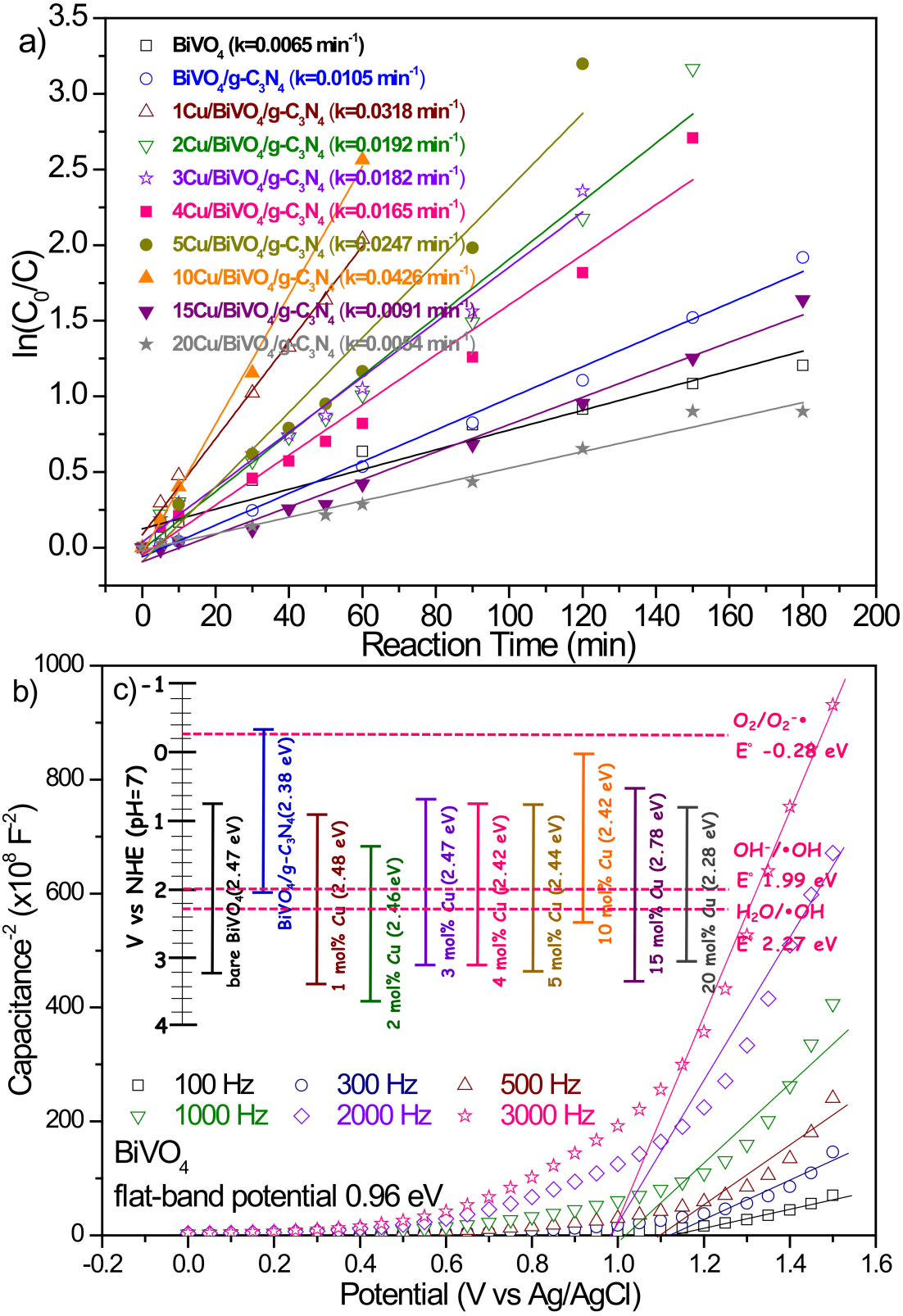

Figure 6. (**a**) Changes of the apparent BPA photodegradation reaction kinetics at different photocatalysts. ((BPA): 20 mg L^{-1}; pH = 10; catalyst concentration of 0.4 g L^{-1}), (**b**) Mott–Schottky plots for $BiVO_4$, (**c**) Energy-level diagram displaying the conduction band and valence band edge positions of $BiVO_4$/g-C_3N_4 nanocomposite photocatalysts with different amounts of copper.

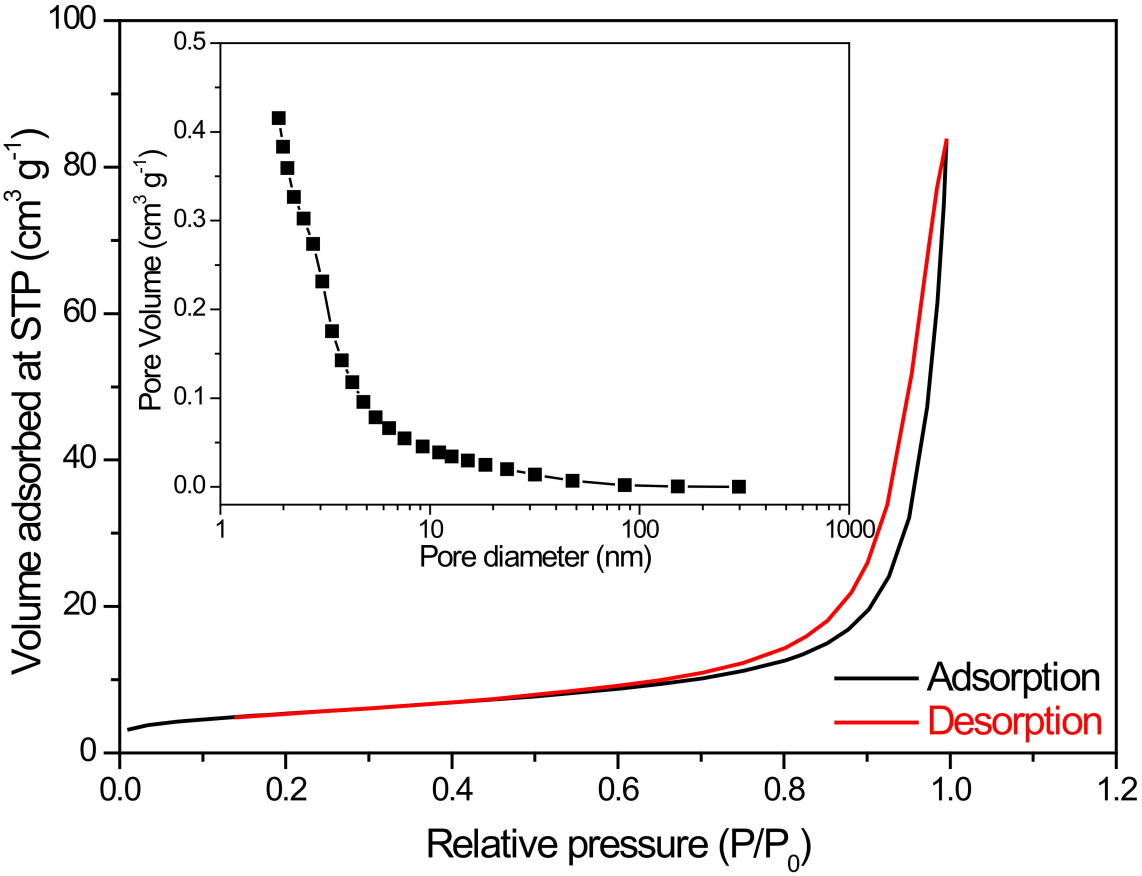

Figure 7. Nitrogen adsorption-desorption and Brunauer-Emmett-Teller (BJH) pore diameter distribution of 10Cu/$BiVO_4$/g-C_3N_4.

Table 1. The surface area of $BiVO_4$/g-C_3N_4 nanocomposite materials with various amounts of copper.

Cu (mol%)	0	1	2	3	4	5	10	15	20
Surface area (m^2/g)	23.1	22.6	22.1	21.5	20.6	20.0	19.4	17.0	15.6

4. Conclusions

$BiVO_4$ nanocomposite photocatalysts were prepared using the sonochemical approach. Cu-doped $BiVO_4$/g-C_3N_4 nanocomposite photocatalysts exhibited a remarkable improvement in degradation performance. The pH values of BPA solution, the dosages of 10Cu/$BiVO_4$/g-C_3N_4, and the various types of $BiVO_4$ nanocomposite material had a great influence on the removal efficiency of BPA. The optimal parameters, such as pH value at 10, photocatalyst dosage of 0.4 g L^{-1}, and 10 mol% Cu-doped $BiVO_4$/g-C_3N_4 photocatalyst, were determined to degrade the initial concentration of 20 ppm bisphenol A, which could be completely removed after 90 min.

Author Contributions: Conceptualization, G.J.-L. and J.J.W.; methodology, all authors; formal analysis, G.J.-L. and X.-Y.L.; investigation, X.-Y.L.; writing—original draft preparation, G.J.-L.; writing—review and editing, J.J.W.; supervision, S.A., C.L., N.L., and J.J.W.; project administration, G.J.-L.; funding acquisition, J.J.W. All authors have read and agreed to the published version of the manuscript.

Funding: This research was funded by the Ministry of Science and Technology (MOST), Taiwan.

Acknowledgments: The authors wish to thank for the financial support by the Ministry of Science and Technology (MOST) in Taiwan under the contract number of MOST-107-2221-E-035 -001 -MY3.

Conflicts of Interest: The authors declare no conflict of interest.

References

1. Tokunaga, S.; Kato, H.; Kudo, A. Selective preparation of monoclinic and tetragonal $BiVO_4$ with scheelite structure and their photocatalytic properties. *Chem. Mater.* **2001**, *13*, 4624–4628. [CrossRef]
2. Kudo, A.; Omori, K.; Kato, H. A novel aqueous process for preparation of crystal form-controlled and highly crystalline $BiVO_4$ powder from layered vanadates at room temperature and its photocatalytic and photophysical properties. *J. Am. Chem. Soc.* **1999**, *121*, 11459–11467. [CrossRef]
3. Zhang, X.; Ai, Z.; Jia, F.; Zhang, L.; Fan, X.; Zou, Z. Selective synthesis and visible-light photocatalytic activities of $BiVO_4$ with different crystalline phases. *Mater. Chem. Phys.* **2007**, *103*, 162–167. [CrossRef]
4. Liu, W.; Cao, L.; Su, G.; Liu, H.; Wang, X.; Zhang, L. Ultrasound assisted synthesis of monoclinic structured spindle $BiVO_4$ particles with hollow structure and its photocatalytic property. *Ultrason. Sonochem.* **2010**, *17*, 669–674. [CrossRef]
5. Martinez Suarez, C.; Hernández, S.; Russo, N. $BiVO_4$ as photocatalyst for solar fuels production through water splitting: A short review. *Appl. Catal. A Gen.* **2015**, *504*, 158–170. [CrossRef]
6. Dong, P.; Xi, X.; Zhang, X.; Hou, G.; Guan, R. Template-free synthesis of monoclinic $BiVO_4$ with porous structure and its high photocatalytic activity. *Materials* **2016**, *9*, 685. [CrossRef]
7. Sun, J.; Wang, C.; Shen, T.; Song, H.; Li, D.; Zhao, R.; Wang, X. Engineering the dimensional interface of $BiVO_4$-2D reduced graphene oxide (RGO) nanocomposite for enhanced visible light photocatalytic performance. *Nanomaterials* **2019**, *9*, 907. [CrossRef]
8. Xie, T.; Li, H.; Liu, C.; Yang, J.; Xiao, T.; Xu, L. Magnetic photocatalyst $BiVO_4$/Mn-Zn ferrite/reduced graphene oxide: Synthesis strategy and its highly photocatalytic activity. *Nanomaterials* **2018**, *8*, 380. [CrossRef]
9. Zhang, B.; Wang, Z.; Peng, X.; Wang, Z.; Zhou, L.; Yin, Q. A novel route to manufacture 2D layer MoS_2 and g-C_3N_4 by atmospheric plasma with enhanced visible-light-driven photocatalysis. *Nanomaterials* **2019**, *9*, 1139. [CrossRef]
10. Smýkalová, A.; Sokolová, B.; Foniok, K.; Matejka, V.; Praus, P. Photocatalytic degradation of selected pharmaceuticals using g-C_3N_4 and TiO_2 nanomaterials. *Nanomaterials* **2019**, *9*, 1194. [CrossRef]
11. Mamba, G.; Mishra, A.K. Graphitic carbon nitride (g-C_3N_4) nanocomposites: A new and exciting generation of visible light driven photocatalysts for environmental pollution remediation. *Appl. Catal. B Environ.* **2016**, *198*, 347–377. [CrossRef]
12. Zhang, Z.; Wang, M.; Cui, W.; Sui, H. Synthesis and characterization of a core–shell $BiVO_4$@g-C_3N_4 photo-catalyst with enhanced photocatalytic activity under visible light irradiation. *RSC Adv.* **2017**, *7*, 8167–8177. [CrossRef]
13. Du, J.; Bao, J.; Fu, X.; Lu, C.; Kim, S.H. Mesoporous sulfur-modified iron oxide as an effective Fenton-like catalyst for degradation of bisphenol A. *Appl. Catal. B Environ.* **2016**, *184*, 132–141. [CrossRef]
14. Yang, L.; Li, Z.; Jiang, H.; Jiang, W.; Su, R.; Luo, S.; Luo, Y. Photoelectrocatalytic oxidation of bisphenol A over mesh of TiO_2/graphene/Cu_2O. *Appl. Catal. B Environ.* **2016**, *183*, 75–85. [CrossRef]
15. Lee, G.J.; Anandan, S.; Masten, S.J.; Wu, J.J. Sonochemical synthesis of hollow copper doped zinc sulfide nanostructures: Optical and catalytic properties for visible light assisted photosplitting of water. *Ind. Eng. Chem. Res.* **2014**, *53*, 8766–8772. [CrossRef]
16. Lee, G.J.; Chen, H.C.; Wu, J.J. Enhancing the photocatalytic hydrogen evolution of copper doped zinc sulfide nanoballs through surfactants modification. *Int. J. Hydrog. Energy* **2019**, *44*, 30563–30573. [CrossRef]
17. Chen, L.; Wang, J.; Meng, D.; Xing, Y.; Tian, X.; Yu, X.; Xu, K.; Wu, X. Effects of citric acid and urea on the structural and morphological characteristics of $BiVO_4$ synthesized by the sol–gel combustion method. *J. Sol-Gel Sci. Technol.* **2015**, *76*, 562–571. [CrossRef]
18. Takahashi, R.; Sato, S.; Sodesawa, T.; Suzuki, M.; Ichikuni, N. Ni/SiO_2 prepared by sol–gel process using citric acid. *Microporous Mesoporous Mater.* **2003**, *66*, 197–208. [CrossRef]
19. Shahi, A.K.; Pandey, B.K.; Gopal, R. PEG mediated solvothermal synthesis of fine ZnS sub-micro and microspheres and their optical properties. *Mater. Lett.* **2014**, *116*, 112–115. [CrossRef]
20. Li, H.; Hong, W.; Cui, Y.; Hu, X.; Fan, S.; Zhu, L. Enhancement of the visible light photocatalytic activity of Cu_2O/$BiVO_4$ catalysts synthesized by ultrasonic dispersion method at room temperature. *Mater. Sci. Eng. B* **2014**, *181*, 1–8. [CrossRef]

21. Safaei, J.; Ullah, H.; Mohamed, N.A.; Noh, M.F.M.; Soh, M.F.; Tahir, A.A.; Ludin, N.A.; Ibrahim, M.A.; Isahak, W.N.R.W.; Teridi, M.A.M. Enhanced photoelectrochemical performance of Z-scheme g-C_3N_4/$BiVO_4$ photocatalyst. *Appl. Catal. B Environ.* **2018**, *234*, 296–310. [CrossRef]
22. Bautista-Toledo, I.; Ferro-Garcia, M.A.; Rivera-Utrilla, J.; Moreno-Castilla, C.; Vegas Fernandez, F.J. Bisphenol A removal from water by activated carbon effects of carbon characteristics and solution chemistry. *Environ. Sci. Technol.* **2005**, *39*, 6246–6250. [CrossRef] [PubMed]
23. Tay, K.S.; Rahman, N.A.; Abas, M.R.B. Degradation of bisphenol A by ozonation: Rate constants, influence of inorganic anions, and by-products. *Maejo Int. J. Sci. Technol.* **2012**, *6*, 77–94.
24. Kuo, C.Y.; Wu, C.H.; Lin, H.Y. Photocatalytic degradation of bisphenol A in a visible light/TiO_2 system. *Desalination* **2010**, *256*, 37–42. [CrossRef]
25. Lee, G.J.; Wang, J.C.; Wu, J.J. Sonochemical synthesis of Ga-doped ZnS nanoballs with enhanced photocatalytic activity for Orange II dye degradation in wastewater. *Int. J. Nanotech.* **2018**, *15*, 804–815. [CrossRef]
26. Lee, G.J.; Chen, H.C.; Wu, J.J. (In, Cu) Co-doped ZnS nanoparticles for photoelectrochemical hydrogen production. *Int. J. Hydrog. Energy* **2019**, *44*, 110–117. [CrossRef]
27. Lee, G.J.; Hou, Y.H.; Liu, N.; Wu, J.J. Enhanced photocatalytic hydrogen and methane evolution using chalcogenide with metal ion modification via a microwave-assisted solvothermal method. *Catal. Today* **2019**, in press. [CrossRef]